Exploring pretopological phases of matter in coupled wires of bosons

Andreas Haller,[1] Apollonas S. Matsoukas-Roubeas,[2] Yueting Pan,[3] Matteo Rizzi,[4,5] and Michele Burrello[2]

[1] *Institute of Physics, Johannes Gutenberg University, D-55099 Mainz, Germany*
[2] *Niels Bohr International Academy and Center for Quantum Devices, University of Copenhagen, Lyngbyvej 2, 2100 Copenhagen, Denmark*
[3] *Center for Advanced Quantum Studies, Department of Physics, Beijing Normal University, 100875 Beijing, China*
[4] *Forschungszentrum Jülich, Institute of Quantum Control, Peter Grünberg Institut (PGI-8), 52425 Jülich, Germany*
[5] *Institute for Theoretical Physics, University of Cologne, D-50937 Köln, Germany*

Introduction.– The experimental investigation of ultracold atomic gases has developed in the last years with remarkable stride. Ultracold atom simulators have been adopted to examine several many-body quantum problems, with the opportunity of tuning the ratio between their interactions and kinetic energies and to trap atomic gases in different geometries. In this context, the study of ladder geometries generated through optical lattices offer the possibility of testing the behavior of quantum systems at the border between one– and two–dimensional systems [3]. Their kinetic energy is firmly one-dimensional, but the presence of plaquettes around which the atoms move allows for the introduction of artificial gauge potentials with non-trivial effects.

In the last years, the effects of these artificial magnetic fluxes have been tested for ladder geometries with a transverse direction defined either in real or "synthetic" dimension [7]. In the latter case, an inner degree of freedom of the atoms is used to represent the transverse coordinate, thus the different legs, in the ladder. Synthetic dimensions offer, in this way, the possibility of defining both sharp edges and artificial gauge fluxes with suitable Raman couplings [15].

The introduction of artificial gauge potentials breaks, in general, time–reversal symmetry, and allows for the onset of helical many-body states, characterized by the appearance of a net chiral current running in counterpropagating directions at the edges of the ladder. Such phenomena have been investigated for both fermionic [30, 35, 40, 41] and bosonic [22, 60] non-interacting gases.

Such experimental setups are currently at the focus of great attention, due to their non-trivial behavior reminiscent of both superconducting [50] and quantum Hall systems [19, 28, 31, 64], and the possibility of engineering interacting topological phases of matter [4, 5, 33, 43, 46, 63]. In particular, these systems are characterized by several commensuration effects. The first kind of commensuration is related to the physics of Mott insulators and appears for commensurate ratios between the number of particles and sites in the ladder [13, 16, 20, 36, 53, 59]. The second kind concerns the ratio between the total artificial magnetic flux enclosed by the ladder and the number of plaquettes in the geometry: several non-trivial phases corresponding to crystals of magnetic vortices alternate when increasing the flux per plaquette at fixed particle density [9, 25–27]. A third, and more elusive, kind of commensuration has been at the center of an intensive study in the last years and it is related to the ratio between the number of particles and magnetic fluxes. For several fractional values of this ratio, suitable repulsive interactions among the atoms cause the onset of partially gapped states, characterized by a helical current. For both fermions and bosons, it has been showed that many of these helical many-body states are indeed the one-dimensional ladder limit of fractional quantum Hall states [11, 12, 29, 51, 52, 55, 56, 61, 65]. They can be considered as pre-topological one-dimensional chiral states. (Please, add all your favourite references in this paragraph)

The physics of these many-body states can be understood in terms of specific resonances between the modulation length of the density of particles and the modulation of the hopping phases determining the external fluxes. In particular, bosonization techniques allow us to understand through semiclassical approximations the fermionic states appearing at filling factor $1/3$ and the bosonic states at filling factor $1/2$ as Laughlin-like pretopological states.

In this work, we focus on the case of 2-leg ladders of bosonic atoms at filling factor $\nu = 1$. Similarly to their fermionic counterpart at $\nu = 1/2$ [29], these states cannot be discussed in terms of a simple semiclassical approximation due to the competition of several operators becoming resonant, and thus relevant, for this specific ratio.

Two–dimensional spinless bosonic systems in Hofstadter-Hubbard models in ladder geometries at $\nu = 1$ have already been numerically studied [32, 38], and it was pointed out that for this specific ratio and certain ranges of the hopping parameters, signatures of a second-incommensurability appear in the correlation functions [18, 48, 49]. A systematic analysis of the appearance and characterization of gaps in this system, however, is still missing.

In this work we fill this gap, and we discuss in detail the physics of this system through bosonization and matrix–product–state simulation. We show, in particular, that helical states appear in a ladder of hardcore bosons. With suitable choices of the interleg interactions,

the signatures of these states, and their gaps, are considerably larger than their fermionic counterpart at filling $\nu = 1/2$. This opens the path for an experimental study of these strongly correlated and helical phases of matter: our simulations and analysis confirm indeed that energy gaps can be opens in synthetic dimension bosonic ladders with contact interactions only, which is the most realistic scenario for atoms trapped in optical lattices.

We will discuss the possible phases of matter characterizing this system in the limit of weak tunneling along the rungs and we will investigate in detail the main correlation functions and entanglement properties of the system.

I. THE MODEL

Ladder models of ultracold bosons trapped in optical lattices have been experimentally realized with rubidium gases both in spacial ladders [3], by using optical superlattices to isolate single two-leg ladders, and in synthetic dimensions [22, 60]. In both cases, suitable pairs of Raman lasers allow to engineer an effective long-time dynamics of the system described by a low-energy tight-binding Hamiltonian characterized by position–dependent phases in the hopping amplitudes of the atoms. The resulting artificial gauge flux χ in each plaquette depends on the recoil momentum of the Raman lasers and can be varied by tuning the angle between the Raman lasers (see, for example, the experiments [1, 2, 45]).

In this work, we focus on the case of ultracold bosons trapped in a two-leg ladder geometry (see Fig. 1a). Their long-time dynamics is described by an interacting Hamiltonian of the form:

$$\mathcal{H} = \mathcal{H}_0 + \mathcal{H}_U + \mathcal{H}_\perp \,, \tag{1}$$

where $\mathcal{H}_0$ represents the kinetic energy of the atoms, whereas $\mathcal{H}_U$ and $\mathcal{H}_\perp$ define respectively the intraleg and interleg repulsive interactions. We consider a ladder geometry with L rungs and a gas of N atoms.

A. The single–particle physics

We begin our analysis from the single–particle features of the model. The kinetic energy $\mathcal{H}_0$ is given by two hopping terms

$$\mathcal{H}_0 = \mathcal{H}_t + \mathcal{H}_\Omega \,, \tag{2}$$

describing a tight-binding model of spinless bosonic particles hopping in the ladder geometry. Our model is characterized by an intraleg tunneling amplitude t and an interleg hopping Ω (see Fig. 1):

$$\begin{aligned} \mathcal{H}_t &= -t \sum_{x=1}^{L-1} \sum_{y=\pm 1} b^\dagger_{x,y} b_{x+1,y} \mathrm{e}^{i\frac{\chi y}{2}} + \text{H.c.}\,, \\ \mathcal{H}_\Omega &= -\Omega \sum_{x=1}^{L-1} b^\dagger_{x,\uparrow} b_{x,\downarrow} + \text{H.c.}\,. \end{aligned} \tag{3}$$

Hereafter we set the lattice spacing $a = 1$ for simplicity; the pseudospin index $y = \pm 1$, or, equivalently, $y = \uparrow, \downarrow$, labels the transverse direction distinguishing two legs of the ladder, and the bosonic annihilation/creation operators $b_{x,y}/b^\dagger_{x,y}$ satisfy the bosonic commutation algebra. We have chosen a gauge which preserves the translational invariance along the x direction, and the hopping phases along this direction define an artificial magnetic flux per plaquette $\chi = \oint \vec{A} d\vec{l}$ defined by the counterclockwise Aarhonov–Bohm phase acquired by an atom moving along any of the ladder plaquettes.

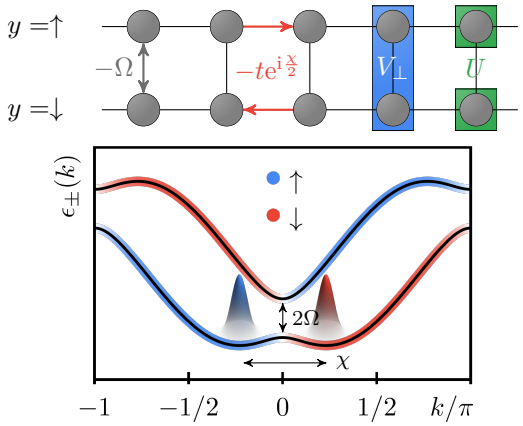

FIG. 1. (a) Graphical representation of the model Hamiltonian. Arrows represent the tight binding terms in Eq. (3) and density-density interactions of Eq. (5) are depicted by colored boxes. (b) Band structure with polarization (in colors) for $\Omega/t = 0.25$. The partial gap induced by inter-wire transitions is of size 2Ω (Update to $y = \pm 1$. I suggest also to remove the mesh of the Gaussians, since we are 1D and not 2D and they may generate confusion. What do you think?).

In a translational invariant case, the single–particle Hamiltonian $\mathcal{H}_0$ can be rewritten in momentum space:

$$\mathcal{H}_0 = -\sum_k \boldsymbol{b}^\dagger_k \begin{pmatrix} 2t\cos(k+\chi/2) & \Omega \\ \Omega & 2t\cos(k-\chi/2) \end{pmatrix} \boldsymbol{b}_k \tag{4}$$

where $\boldsymbol{b}_k = (b_{k,\uparrow}, b_{k,\downarrow})^\intercal$ is a two-component spinor.

The spectrum of the Hamiltonian (4) is depicted in Fig. 1 (b) for a small value of Ω/t; it matches the typical spectrum of one-dimensional systems characterized by a spin-orbit coupling (whose role is played by χ in $\mathcal{H}_t$) and the Zeeman splitting Ω. $\mathcal{H}_t$ defines indeed two cosine dispersions, for pseudospin $y = \uparrow$ and $y = \downarrow$, which are displaced in momentum space by the flux χ. In the case

of bosons, the particles condense around the two minima of these dispersions and their momentum, which can be measured through time–of–flight experiments, is locked to their spins, thus with the leg (see, for example, [22, 60]).

The role of $\mathcal{H}_\Omega$ is to open a gap 2Ω at $k = 0$. This gap can be interpreted as the bulk gap of a quantum Hall system in the one–dimensional ladder limit [19]. When Ω exceeds a threshold $\Omega_c(\chi)$, the minimum of the energy dispersion becomes non-degenerate at $k = 0$ and the system becomes a superfluid whose atoms are aligned in the x direction of the pseudospin. For non-interacting bosonic systems, this corresponds to the Meissner phase characterized by a chiral current proportional to the flux χ [3].

The non-interacting system is indeed characterized by two main phases: the Meissner phase appearing at small fluxes and sufficiently large interleg tunneling Ω, and a vortex phase appearing at larger fluxes or smaller values of Ω [3, 50].

The introduction of repulsive interactions strengthen the Meissner phase and allows for the appearance of several partially gapped and strongly correlated states in the vortex phase.

B. Introducing the interactions

In ultracold atom experiments repulsive contact interactions among atoms are common. For a realization of the ladder model in synthetic dimension, atoms whose position differs only by the transverse y coordinate are actually located on the same physical position. Therefore contact repulsions are represented by the following density-density interactions

$$\begin{aligned}\mathcal{H}_U &= \frac{U}{2}\sum_x n_{x,y}(n_{x,y}-1)\,,\\ \mathcal{H}_\perp &= V_\perp \sum_{x,y} n_{x,y}n_{x,y+1}\,,\end{aligned} \tag{5}$$

with $n_{x,y} = b^\dagger_{x,y}b_{x,y}$. Such interactions have the potential to drive the system from the vortex to different helical phases, if the total density n is commensurate to the flux χ [12, 19, 52].

We observe, in particular, that for ultracold atoms trapped in optical lattices the ratio between interaction and kinetic energy can be varied by changing the amplitude of the trapping lasers which define the depth of the trapping lattice.

Concerning the ratio between U and $V_\perp$, tunable intraspecies and interspecies interactions can be achieved through the introduction of suitable magnetic fields via Fano-Feshbach resonances [17]. For example, for Rb gases in their ground state manifold, U and $V_\perp$ are typically comparable, with scattering length differing by only a few percent. However the related scattering length can be considerably varied by using Fano-Feshbach resonances [17, 42].

For the remainder of this work, and, especially, in our numerical simulations, we will mostly consider the ladder hard–core bosonic (HCB) scenario, in which $U/t \to \infty$ is the dominating interaction which excludes any double occupation of a single site (x, y), i.e. $n_{x,y} \leq 1$. We will consider instead a tunable interspecies interaction $V_\perp$.

II. EFFECTIVE LOW–ENERGY DESCRIPTION OF THE MODEL

To study the physics of the interacting system at zero temperature we set up a low-energy description of the system in the continuum limit based on bosonization [23, 24]. In particular, to examine the chiral states appearing at commensurate values of the filling factor $\nu = \pi N/L\chi$, it is necessary adopt the following bosonization identity for bosons [14], which accounts for higher harmonics of the density modulations:

$$b^\dagger_{x,y} \to \Psi^\dagger_y(x) \sim \sum_{p\in 2\mathbb{Z}} \beta_p \mathrm{e}^{i[(pk_0+y\chi)x - p\theta_y(x) - \varphi_y(x)]}\,; \tag{6}$$

here $k_0 = \pi N/(2L)$ is the wavevector associated to the density modulations and we introduced two pairs of dual fields that satisfy the commutation algebra $\left[\theta_{y'}(x'), \varphi_y(x)\right] = i\pi\delta_{yy'}\Theta(x'-x)$. The fields θ_y and φ_y are associated to the charge and current fluctuations of the particles in the two legs and, in particular, the density operator can be approximated with $n(x, y) \approx (k_0 - \partial_x\theta_y(x))/\pi$, whereas the current density j_y is proportional to $\partial_x\varphi_y$. Finally, β_p is a set of non-universal parameters, and, for our purposes, we will set$\beta_0 = 1$, $\beta_{\pm 2} = 1/2$, whereas all the other β's are set to 0 (see Appendix A for more detail).

The general effective interacting Hamiltonian is mapped into a two-species Luttinger liquid (with central charge $\mathsf{c} = 2$) (Observe that here I changed the font for the central charge to avoid confusion with the charge sector), which can be described in terms of two decoupled charge c and spin s sectors. Additionally, the interleg tunneling Ω and repulsion $V_\perp$ determine the presence of additional interactions, which can be cast into a generalized sine-Gordon form. The effective bosonized Hamiltonian is derived in Appendix A and assumes the form:

$$\begin{aligned}\mathcal{H} = &\sum_{a\in\{c,s\}} \int \frac{\mathrm{d}x}{2\pi}\left[u_a K_a(\partial_x\varphi_a(x))^2 + \frac{u_a}{K_a}(\partial_x\theta_a)^2\right]\\ &+ \int \mathrm{d}x\left[h\cos(2\sqrt{2}\theta_s) + g\mathrm{e}^{i(2k_0-\chi)x}O_g(x)\right]\end{aligned} \tag{7}$$

with $\mathcal{O}_g(x) = \mathrm{e}^{i\sqrt{2}(\theta_c+\theta_s-\varphi_s)} + \mathrm{e}^{i\sqrt{2}(\theta_c-\theta_s-\varphi_s)} + \mathrm{H.c.}$ (see also [18, 49]). The operator $\mathcal{O}_g$ is, in general, fast–oscillating, such that it averages to a non-zero value only if its phase lose the fast–oscillating behavior, thus the system approaches the resonance $2k_0 = \chi$, corresponding

to the commensurate filling factor $\nu = 1$. In the Hamiltonian (7) we neglected other fast-oscillating terms that are responsible for the onset of different pre-topological states (see, for example, [11, 19, 51]) but are irrelevant in proximity of $\nu = 1$. Additional terms, less relevant in the renormalization group (RG) sense, have been neglected as well.

The parameters u_a and K_a in the Hamiltonian (7) respectively represents the velocities of the bosonic modes and the Luttinger parameters of the model sectors $a = c, s$. Since the interactions we consider are only of the density-density kind, the value of the superfluid stiffness is fixed and $u_a K_a = u_0 = 2t \sin k_0$.

Finally, the values of the (bare) coupling constants h and g depend on $V_\perp$ and Ω respectively and can be approximated as:

$$h = \frac{k_0^2 V_\perp \beta_2^2}{2\pi^2}\,, \quad g = -\frac{\Omega \beta_2 k_0}{2\pi^2}\,; \tag{8}$$

see Appendix A for more detail.

Differently from the pre–topological Laughlin–like states [11, 19, 51], the physics of bosons at $\nu = 1$ is dictated by the interplay of the non-commuting operators appearing in $\mathcal{O}_g$ and in the h–term. The g–term, in particular, require special attention: its components have the same amplitudes and scaling dimension, such that a simple semiclassical approach may not suffice for a clear understanding of the behavior of this system in the thermodynamic limit. In the following we resort to a second-order RG analysis, in analogy with the fermionic ladder models at filling $\nu = 1/2$ [29], and numerical simulations based on matrix product states (MPS).

III. RENORMALIZATION GROUP ANALYSIS

A first insight of the possible thermodynamical phases and properties of the model is given by a simple scaling analysis of the interactions in the effective Hamiltonian (7).

The linear combination of fields appearing in the two terms within the $\mathcal{O}_g$ operator and in the h interaction do not commute. Therefore, in the ground states of the model, each of these three terms favors the minimization of different combinations of densities and currents which are not compatible with each other. Both the contributions in $\mathcal{O}_g$ are characterized by a scaling dimension $D_g = \left(K_c + K_s + K_s^{-1}\right)/2$ and, having the same coupling constant, none of the two can dominate over the other. The scaling dimension of the h term is instead $D_h = 2K_s$, such that this operator would be always irrelevant, in the RG sense, for repulsive contact interaction for which $K_s > 1$.

The form of the Hamiltonian (7) suggests the potential existence of three phases.

The first is a Luttinger phase in which both the interactions are irrelevant. It corresponds to the vortex phase of the ladder, in which both the charge and spin sectors are gapless and all the two-point correlation functions decay algebraically.

The second phase is the phase dominated by the h–interaction. Hereafter, we will call it h–phase. In this phase the spin sector is gapped and the charge sector is gapless, therefore the central charge decreases to $\mathsf{c} = 1$. The h-phase, semiclassically, corresponds to the situation in which the field θ_s is pinned to one of the minima of the h–interaction. As a consequence, the pseudospin fluctuations and rung current on the ladder are suppressed in the bulk of the system. However, it is important to remark that, for finite systems with open boundary conditions, a rung current appears at the edges of the system. In the numerical systems we will analyze in the following, the gap in the spin sector which characterizes this phase are small and, in particular, we expect a correlation length comparable with the system size. Under these conditions, the system is far from its thermodynamic limit and the rung current can easily be sizable also in its bulk (if we wish we may add this figure in an appendix). We remark that this phase is qualitatively different from the Meissner phase appearing at small fluxes since, in the Meissner phase, it is the rung current being ordered rather than the pseudospin density, corrsponding to the field φ_s being pinned to a semiclassical minimum.

The third phase is the one in which the operator $\mathcal{O}_g$ dominates, and we will refer to it as the g–phase. The study of this phase is less straightforward and its characteristics can be intuitively understood through a mean-field analysis based on the mapping into a Wess-Zumino-Witten (WZW) model (see, for example [24]) proposed in [18, 49]. We sketch in the following the key elements to gain insight into this phase. At the mean-field level, we can separate the contribution of the $\mathcal{O}_g$ operator into the operators $o_c = e^{i\sqrt{2}\theta_c}$ acting on the charge sector, and $o_{s,\pm} = e^{i\sqrt{2}(\varphi_s \pm \theta_s)}$ acting on the spin sector. Assuming that the operators $o_{s,\pm}$ acquire a non-zero expectation value $\langle o_{s,\pm}\rangle$, the operator o_c opens a gap in the charge sector and suppresses the fluctuations of the charge density. The situation is different in the spin sector: the operators $\langle o_{s,\pm}\rangle$ can be mapped into the chiral current operators J_R^y and J_L^y of a WZW model describing the spin sector. With an additional mapping from this WZW model into a rotated Luttinger liquid Hamiltonian [18, 49], it is possible to show that these operators do not open a gap in the spin sector for small values of their coupling constants. This can be understood by considering that the current operator $J_R^y + J_L^y$ constitutes a perturbation proportional to $\partial_x \tilde{\varphi}_s$ in the rotated Luttinger liquid: such perturbation shifts the expectation value $\langle \partial_x \tilde{\varphi}_s \rangle$, thus it introduces incommensurability without opening a spin gap [49].

In conclusion, mean–field arguments suggest that the g–phase is a phase with central charge $\mathsf{c} = 1$ corresponding to a gapped charge sector and a gapless spin sector. Such mean–field analysis neglects the interactions mixing the spin and charge sectors, and may provide only an approximate description of the g–phase. In partic-

ular, they were proposed in [18, 49] to investigate the appearance of a second incommensurability effect in the correlation functions of the system for values of Ω comparable with t, with ladders typically close or within the Meissner phase. We believe, however, that such analysis can be extended also in our regime for $\Omega \ll t$ and systems with well-separated Meissner and $\nu = 1$ resonances. We mention, however, that for contact interactions only we do not observe the onset of the g–phase in this regime.

The scaling dimensions D_h and D_g allow us to obtain a simplified phase diagram as a function of the Luttinger parameters (dashed lines in Fig. 2): the system is gapless for large values of K_c and K_s (Luttinger/vortex phase); the h–phase appears for small values of K_s, such that the h–interactions is more and more relevant; the g–phase occupies instead a region for small values of K_c and intermediate values of K_s.

Given the complexity of the g–interactions, however, we apply a Wilsonian RG study of the Hamiltonian (7) at second order in the interaction paramaters g and h to obtain a more accurate phase diagram. In Appendix A 2 we derive the following RG differential equations:

$$\begin{aligned}
\frac{\mathrm{d}h}{\mathrm{d}l} &= h(2-D_h) + 2g^2\left(\frac{K_c}{u_c} - \frac{K_s}{u_s} + \frac{1}{K_s u_s}\right), \\
\frac{\mathrm{d}g}{\mathrm{d}l} &= g(2-D_g) - hg\frac{K_s}{u_s}, \\
\frac{\mathrm{d}K_c}{\mathrm{d}l} &= 4\pi g^2\left[\frac{K_c}{u_c^2} + \left(K_s + K_s^{-1}\right)\frac{u_s^2+u_c^2}{2u_c u_s^3}\right]K_c^2, \\
\frac{\mathrm{d}K_s}{\mathrm{d}l} &= -4\pi\left[\frac{2h^2K_s^3}{u_s^2}\right. \\
&\quad \left. + g^2\left(1-K_s^2\right)\left(\frac{u_c^2+u_s^2}{2u_s u_c^3}K_c + \frac{K_s+K_s^{-1}}{u_s^2}\right)\right].
\end{aligned} \tag{9}$$

In Fig. 2 we present a phase diagram obtained from the numerical solution of these RG equations, as a function of the bare initial values of K_c and K_s, and considering the bare values of the coupling constants in Eq. (8) obtained by setting the non-universal parameter $\beta_2 = 1/2$ (see Appendix A). The numerical results are obtained by setting $\Omega = 0.05t$ and $V_\perp = t$ to determine the bare values of g and h.

The phase diagram is determined by setting an upper threshold ($\tilde{\Delta} = t$) and a lower threshold ($\tilde{\delta} = t/100$) to the moduli of g and h. If, during the flow, any of the two coupling constants increases beyond the threshold, we consider that the system reached a strong–coupling (partially gapped) phase at a value of the flow parameter l^* such that $g(l^*)$ or $h(l^*) = \tilde{\Delta}$. Depending on which coupling constant is dominating, we characterize the gapped phase as being of the g or h kind. (In case you like, here we can add a first comment about the gap [see the commented text]. However I discussed the gap also in the next section.) If instead, both the coupling constants drop below the lower threshold, we conclude that the system flows into the Luttinger/vortex phase.

The resulting phase diagram in Fig. 2 must be considered as a qualitative phase diagram valid for small values of the bare parameters in (8): we checked that its features are essentially stable for $V_\perp < 5t$. Above this threshold, non-physical features appear (especially for large values of K_s) that indicate that higher orders of the perturbation theory are not negligible. Furthermore, the behavior of the flow close to the border between the h and g phase cannot be precisely determined: we cannot distinguish whether there is a direct phase transition between these two gapped phases or rather an extended Luttinger region that separates them. Furthermore, the second–order results show that the g–phase is considerably smaller than what expected by the simple first–order scaling analysis, whereas the h and Luttinger phases increase their extension.

The phase diagram in Fig. 2 presents an overview of the possible phases at moderate values of the bare coupling constants g and h. The point $K_s = K_c = 1$ represents the ladder of hardcore bosons with $V_\perp = 0$, which lies in proximity of the phase transition between the Luttinger and the h–phase. In such scenario, the h–interaction is indeed marginal and the role of the resonant g–interaction becomes crucial in determining the thermodynamic behavior of the system. This is due to the second order term, proportional to g^2 which enhances the value of h during the RG flow. Away from the resonance $\chi = 2k_0$, g averages to 0, and h is suppressed for repulsive interactions, which yield $K_s > 1$ (see Eq. (10) below). At resonance, instead, the coupling g not only can give rise to the g–phase, but it also strengthen the h–phase.

To gain a more realistic insight of the system we restric our discussion to the case of hard-core bosons on the ladder geometry. Based on the mapping of the single leg subsystems into fermions (see Appendix A) we can approximate the bare values of the Luttinger parameters as:

$$\begin{aligned}
K_c(0) &= \sqrt{\frac{2\pi t\sin(k_0 a)}{2\pi t\sin(k_0 a) + V_\perp}}, , \\
K_s(0) &= \sqrt{\frac{2\pi t\sin(k_0 a)}{2\pi t\sin(k_0 a) - V_\perp}}.
\end{aligned} \tag{10}$$

These relations rely on the limit $V_\perp \ll t$ and, as we will discuss in the next sections based on tensor network simulations, these approximations underestimate K_c for large $V_\perp$ (and overestimate K_s?: I am not sure about the values of K_s; probably we should cut this.) (see Fig. 5). In particular, in the limit $\Omega \to 0$ the model can be mapped into a spinless fermionic Hubbard model [19] and $K_c \to 1/2$ for $V_\perp \to \infty$. This lower limit, however, depends on Ω.

Therefore, for the model of hard–core bosons, all the bare parameters K_c, K_s, g and h are determined based on the value of $V_\perp$, and, when varying $V_\perp$ from 0 to ∞, the system will be characterized by a trajectory in a three-dimensional phase diagram as a function of K_c, K_s and $V_\perp$. With respect to Fig. 2, we observe that for larger

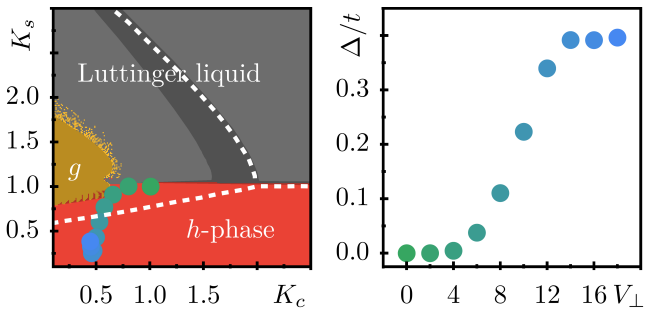

FIG. 2. (a) Expected phases at $\chi/\pi = n$ for different values of K_s and K_c. The colored regions correspond to the numerical outcomes of the second order RG flow for $V_\perp = t$ (see main text): the gray region depicts the Luttinger/vortex phase, the yellow region corresponds to the g–phase and the red region to the h–phase (the shaded regions correspond to slowly converging and divergent regions of the RG equations) . The dotted lines signal the boundaries of the phases as obtained by a first-order scaling analysis: $D_{g/h} > 2$ (Luttinger), $D_g < 2, D_h$ (g-dominated), $D_h < 2, D_g$ (h-dominated). From first to second order the g–phase significantly shrinks. The shaded region marks large values of the maximum RG-evolution $l^* > 10$ for which the second-order outcomes are not completely reliable. The central blue circle denotes our numerical starting point of hard core bosons (HCB) forming a vortex phase. Our numerical simulations of the interacting systems are projected onto the the path formed by the circles changing color from blue to black as the amplitude $V_\perp/t$ is increased. The values are extracted from the fitted values of K_s and K_c such as those we present in Fig. 5. (b) Estimate of the gap $\Delta = te^{-l^*}$ computed from second order RG with initial values taken from the MPS simulations. The estimates of the gap are in agreement to the nontrivial change in the correlation functions and chiral current after a critical value of the interaction $V_\perp/t \gtrapprox 6$.

values of $V_\perp$ the g–phase is shifted towards larger values of K_s (Andreas prepared a new section of the phase diagram as a function of $V_\perp$ and K_s for $K_c = 0.5$, we can add it as a novel figure in the main text, or in Appendix B). The white line in Fig. 2 depicts the projection of this trajectory, determined by the MPS simulations in the next sections, over the K_c, K_s plane at $V_\perp = t$.

Based on this trajectory, we predict that the system at $V_\perp = 0$ lies in proximity of the edges between the Luttinger and the two gapped phases, it evolves close to the boundary between the h and g phases for intermediate values of $V_\perp$ and, finally, it develops a larger gap entering deep in the h–phase.

We emphasize, however, that this second–order RG analysis based on Eqs. (8,9) and (10) provides accurate results only for $h < t$, thus for sufficiently small $V_\perp k_0^2$. Therefore, in the next sections we complement the previous RG predictions with the MPS results spanning over a broad range of $V_\perp$.

IV. NUMERICAL RESULTS

In order to obtain quantitative predictions about the behavior of the model for ladders of sizes comparable with realistic experimental scenarios, we simulated the Hamiltonian (1) for $L = 64$ and hard–core bosons, for different values of the rung repulsive interaction $V_\perp$. The simulations were performed through density matrix renormalization group, adopting an matrix product state (MPS) ansatz with open boundary conditions and bond dimensions varying up to ...

A. Chiral current

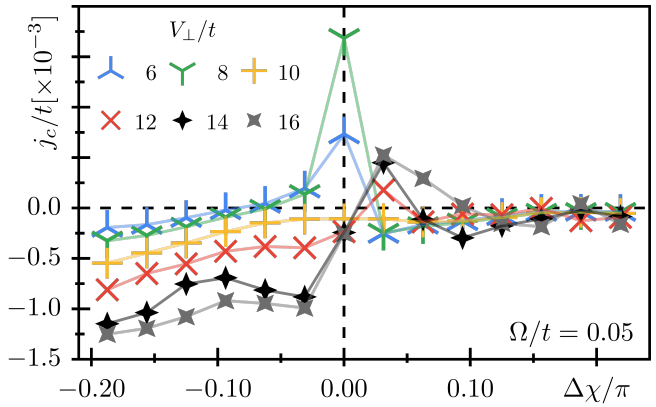

FIG. 3. Chiral current j_c as a function of the magnetic flux $\Delta\chi/\pi = \chi/\pi - n$ for different interaction strengths $V_\perp/t$ for $N = 48$, $L = 64$ and $\Omega = 0.05t$. For large interactions, the spin sector is gapped at integer filling factors imposing the condition $\chi/\pi = n$. As a consequence, we observe a double cusp-signature of the chiral current.

We focus on values of the density of hard-core bosons and flux per plaquette in proximity to the $\nu = 1$ (for example $N = 48$ and $\chi = 3\pi/4$ for $L = 64$) and we vary the interactions $V_\perp$ and the flux χ. In particular we vary the flux in units of $2\pi/L$ because all the observables in the open system display strong and regular oscillations when continuously varying χ. The chosen discretization corresponds to a unit quantum of momentum for translationally invariant chains and is somewhat arbitrary: similar results are obtained by slightly larger/smaller flux variations $2\pi/(L \pm 1)$ which are both equally well justified [quantum of momentum or a flux quantum for Dirichlet-boundary conditioned systems].

Let us observe first the behavior of the chiral current j_c of the system:

$$j_c = i\frac{t}{2L}\sum_x \left(e^{i\frac{\chi}{2}} b^\dagger_{x,\uparrow} b_{x+1,\uparrow} - e^{-i\frac{\chi}{2}} b^\dagger_{x,\downarrow} b_{x+1,\downarrow}\right) + \text{H.c.}\,. \tag{11}$$

Here the chiral current is defined based on the gauge choice in Eq. (3) and we consider its average over the

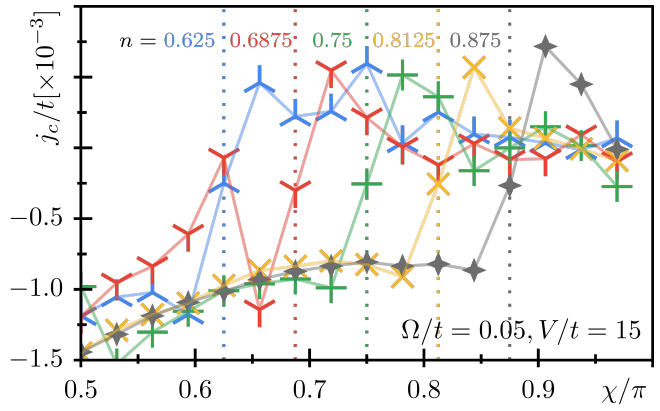

FIG. 4. Chiral current j_c as a function of the magnetic flux χ/π for different average densities $n = N/L$ (different colors and symbols) of the system at $V_\perp/t = 15$ and $\Omega/t = 0.05$. The position of integer filling factor imposes the commensuration $\chi/\pi = n$ and thus shifts the double-cusp signature in the χ-axis.

whole chain length (Andreas, check and modify in case).

Fig. 3 depicts j_c for $N = 48$ as a function of the flux displacement around the resonance $\nu = 1$. For values of $V_\perp < 6t$ (not shown) the chiral current is essentially flat and does not display any discontinuity with respect to the vortex/Luttinger phase. This is compatible indeed with the system being in the Luttinger phase or in very close proximity to it, consistently with the second–order RG results close to $K_c = K_s = 1$ (see Fig. 2). When increasing $V_\perp$ in the approximate range $(6t, 8t)$ the system develops a high peak in the chiral current exactly at the resonance (gray and black curves). We interpret this peak as a feature due to the system evolving towards the critical region at the egde between the h and g phases. By increasing further the interaction, at $V_\perp = 10t$, the current signature flattens again. Finally, for $10t < V_\perp < 18t$ the chiral current develops a stable double cusp pattern, which is an hall mark of the two commensurate-incommensurate phase transitions [21, 23, 54] that separate a (partially) gapped commensurate and chiral phase at the resonance (the h phase) from the gapless vortex phase that dominates when the flux χ is sufficiently displaced from the resonant point (see [11, 19, 52] for the similar signatures of the Laughlin-like phases). We observe that, in this regime, the chiral current cusps are about 4? (to be checked) times larger than the analogous cusps appearing for the $\nu = 1/2$ Laughlin-like states at $\chi = 4k_0$ and $\chi = 2\pi - 4k_0$ (the latter being the particle-hole symmetric state of the Laughlin-like state).

The behavior of the chiral current in the h phase can be deduced by the relation:

$$j_\chi = -\frac{1}{L}\frac{\partial E_{\rm GS}(\chi)}{\partial \chi} \tag{12}$$

in which $E_{\rm GS}$ denotes the ground state energy. If the interaction associated with amplitude h is the dominating term, a gap in the spin sector is formed and the chiral current follows a linear behavior with respect the flux χ between the two cusps and is predicted to cross 0 exactly at the resonance, although the numerical data show a weak background current which is a remnant of the vortex phase.

We verified that, for different particle numbers, the position of the two cusps of the chiral current shift accordingly to the resonance following the relation $\chi = 2k_0$ (see Fig. 4) [check and improve]: the signature of a chiral phase at integer resonance appears indeed for a broad range of particle numbers and its features are visible as long as the $\nu = 1$ resonance is sufficiently separated from the Meissner phase of the system.

(Shall we add anything about large $V_\perp > 18t$?)

Add something about the entanglement properties: we should show here that also the entanglement spectrum has discontinuities in correspondence to the variations of the chiral current

B. Estimate of the Luttinger parameters

To better compare the numerical results with the RG predictions, we must locate the state of the system as a function of $V_\perp$ in the phase diagram obtained by the equations (9) (see the white lines in Fig. 2). To this purpose we must estimate the Luttinger parameters K_c and K_s from the DMRG results. The Luttinger parameters determine most of the features of the ground state of the system, including its spin and charge fluctuations, the decay of its two–point correlation functions and even the dynamics of its excitations.

The first estimates we derive for the Luttinger parameters are obtained by fitting the bipartite charge and spin fluctuations [58]. In particular, we define

$$\mathcal{F}^{c/s}(\ell) = \langle [N^{c/s}(\ell)]^2 \rangle_{\rm conn.} \tag{13}$$

where we introduced the total number of particles / the total magnetization $N^{c/s}$ in a bipartition of size ℓ. In bosonization, the leading order of these fluctuations read

$$\mathcal{F}^{c/s}(\ell) = \frac{2}{\pi^2}\langle \left[\theta_{c/s}(\ell) - \theta_{c/s}(0)\right]^2 \rangle \tag{14}$$

and depend thus on the correlations of the density fields $\theta_{c/s}$. If the corresponding sector is gapless, bipartite fluctuations follow a logarithmic dependence (see Appendix A 3):

$$\mathcal{F}^{a}(\ell) \propto \frac{K_a}{\pi^2}\ln[d(\ell|L)] + f_a\,, \tag{15}$$

(About the spin sector, I have many doubts.) Here $d(\ell|L)$ labels the chord distance of an open boundary system:

$$d(\ell|L) = \frac{L}{\pi}|\sin(\pi\ell/L)|. \tag{16}$$

The function $f_{c/s}$ accounts for the total charge/spin fluctuation of the system, which is related to the $U(1)$ gauge transformations in the corresponding sectors: if the total charge/magnetization is conserved, $f_{c/s} = \varepsilon$, but if it is broken, it constitutes a linear contribution in the bipartition length $f_{c/s} = \gamma + f_0 \ell$, which equally distributes the total fluctuations on each site.

From the fits of the DMRG results we derive that the value of K_c remains essentially constant as a function of the flux χ (see Fig. 5 d). This is the expected behavior across the Meissner-vortex phase, since the Meissner phase presents a gap in the spin sector only. When considering the integer resonance at $\chi = 2k_0$, the independence of K_c from the flux χ suggests that also in this case the physics at the resonance is dictated by a gap in the spin sector only. This is the first indication that, at $\nu = 1$ and sufficiently large $V_\perp$, the system enters the h–phase, whereas the g–phase, expected to have a gapped charge sector, is not reached.

Interestingly, we find also a signature of the pinned spin sector by fitting the constant f_0 in the fluctuations of the total magnetization: it shows a sharp increase in the Meissner and the resonant state at filling $n = \chi/\pi$.

Considering the system exactly at the resonance, we can therefore fit the values of the Luttinger parameters as a function of $V_\perp$ based on Eq. (15). The results are used to define the dots of the physical trajectory presented in Fig. 2. The values of $V_\perp$ and of the fitted Luttinger parameters can then be adopted as initial conditions of the RG flow determined by the equations (9). The numerical solutions of these flow equations allows for an estimate of the gap of the system: we can indeed determine the value l^* of the flow parameter at which one of the coupling constants reaches the upper threshold $\tilde{\Delta} = t$. The gap may be estimated as $\Delta \approx t e^{-l^*}$ and its value is represented in Fig. 2b as a function of $V_\perp$. The behavior of the gap is in striking agreement with the previous analysis of the measured chiral current: the gap is negligible for $V_\perp < 6t$ and it opens in correspondence of the first peak of the chiral current at $V_\perp \sim 6t, 8t$. This suggests that the system lies in the Luttinger/vortex phase (or inside the h–phase but very close to the boundary with the gapless region) until it reaches the region between the h and g phases for $V_\perp \sim 6t, 8t$. For stronger interactions, the predicted gap Δ remains sizable, consistently with the system entering well within the h–phase. To be checked and revised.

C. Correlations

In order to better characterize the gapped phase at the resonance, we study the decay of several two–point correlation functions. indeed, the correlation function allow us to easily distinguish the Meissner and vortex phases, and provide further indications that the system develops a gap in the spin sector at the integer resonance. In particular, the following set of observables is studied

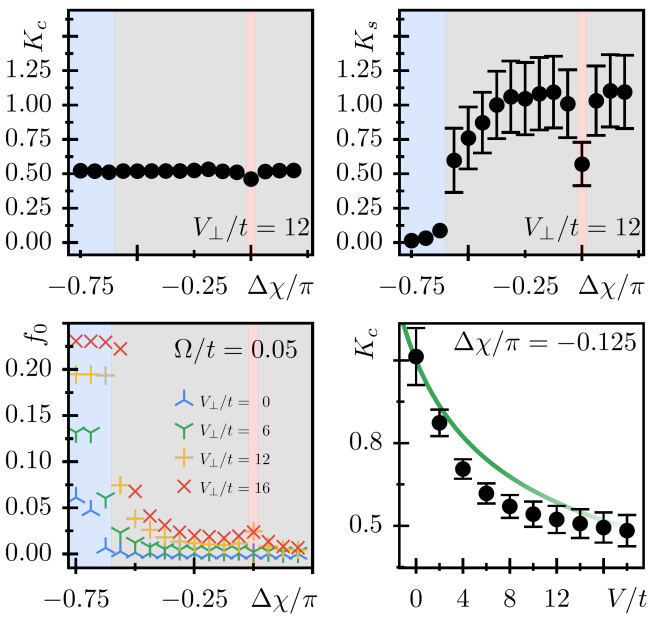

FIG. 5. Luttinger liquid parameters for hard core bosons, $\Omega/t = 0.05$ and $n = N/L = 48/64$. Panels (a/b) show $K_{c/s}$ for $V_\perp/t = 8$, fitted from the fluctuations of the total density / magnetization $N_{c/s}(\ell)$. We see clearly the pinning of the spin fields in the Meissner phase (shaded in blue), and in the resonance at $\chi/\pi = n$ (shaded in red). The pinning of the spin field is further confirmed by fits of the constant f_0. The results agree very well with the prediction of the h-dominated phase given in Fig. 2.

in Fig. 6

$$C_s(i,j) = \langle b^\dagger_{i,+1/2} b_{i,-1/2} b^\dagger_{j,-1/2} b_{j,+1/2} \rangle - \langle b^\dagger_{i,+1/2} b_{i,-1/2} \rangle \langle b^\dagger_{j,-1/2} b_{j,+1/2} \rangle \quad (17)$$

$$C_c(i,j) = \langle b^\dagger_{i,+1/2} b^\dagger_{i,-1/2} b_{j,-1/2} b_{j,+1/2} \rangle, \quad (18)$$

$$G_{y,y'}(i,j) = \langle b^\dagger_{i,y} b_{j,y'} \rangle. \quad (19)$$

We rewrite them in bosonized form and find

$$C_s(x,x') \propto \mathrm{e}^{-\langle [\varphi_s(x) - \varphi_s(x')]^2 \rangle} f_s(x,x') \quad (20)$$

$$C_c(x,x') \propto \mathrm{e}^{-\langle [\varphi_c(x) - \varphi_c(x')]^2 \rangle} (1 + f_c(x,x')) \quad (21)$$

$$G_{y,y'}(x,x') \propto \mathrm{e}^{-\frac{1}{2}\langle [\varphi_y(x) - \varphi_{y'}(x')]^2 \rangle} (1 + g_{y,y'}(x,x')) \quad (22)$$

in which $f_{s/c}$ and $g_{y,y'}$ denote the corrections to the leading order. In particular, the leading order is obtained by separating the $p = 0$ contribution from higher harmonics $p \neq 0$ in Eq. (6).

I moved the equations of the correlations of the bosonic fields in Appendix A 3. There are several things I am not sure about concerning the spin sector.

It is most convenient to plot the above correlation functions as a function of the renormalized chord distance

$$\tilde{d}(x,x') = \frac{d(x - x'|2L) d(x + x'|2L)}{\sqrt{d(2x|2L) d(2x'|2L)}}, \quad (23)$$

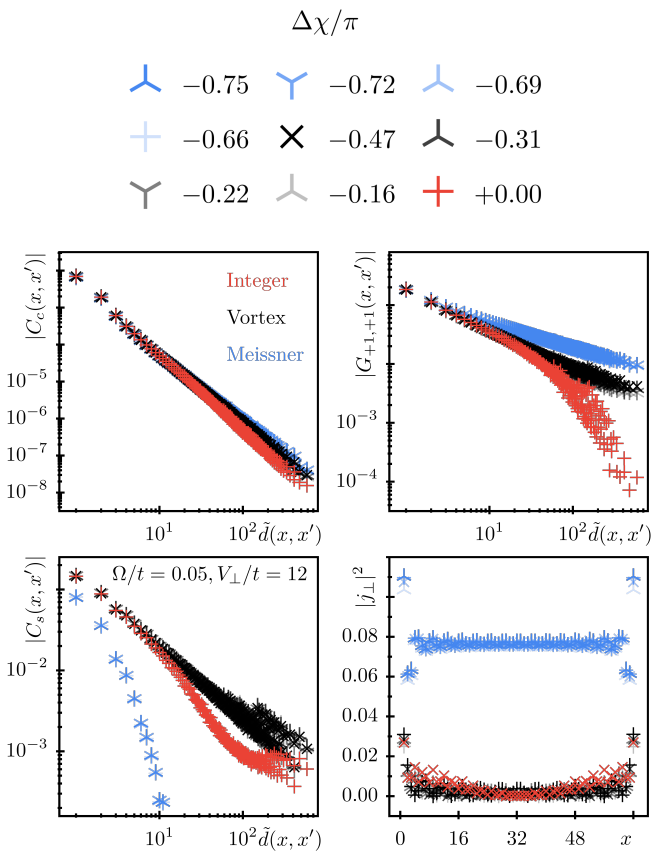

FIG. 6. (a)-(c) Correlation functions $C_{c/s}$ and $G_{+1,+1}$ given by Eq. (22) versus renormalized chord distance $\tilde{d}$ given in Eq. (23). We see a clear pinning of φ_s in the Meissner phase and at $\chi/\pi = n$, as visible by the exponential behavior in C_s at small and intermediate distances. The local expectation values of the rung current is depicted in panel (d).

which highlights the leading order decay caused by the momentum field expectation values.

In particular, the connected part of C_s shows the expected behavior: it follows an algebraic decay ($C_s \propto \tilde{d}^{-1/K_s}$) in the Vortex- and shows an exponential tail in the h-phase at filling $\nu = 1$ due to the gap in the spin sector (from the pinning of θ_s). In the Meissner phase instead, φ_s is pinned and C_s quickly approaches a constant (up to exponential corrections from subleading terms). In contrast to C_s, C_c decays algebraically everywhere ($C_c \propto \tilde{d}^{-1/K_c}$), with no signatures of any exponential tails. This is expected as the charge sector remains always gapless. Finally, the intra-wire Green's function $G_{y,y}$ shows a clear exponential tail in the h-phase, in agreement to our statements above. In the Meissner phase instead, we find $G_{y,y} \approx G_{y,-y} \propto \tilde{d}^{-1/(4K_c)}$ which is predicted by the leading order of Eq.(22).

Interactions	Laughlin $\nu = 1/3$	Laughlin $\nu = 1/2$	h-phase	g-phase
Fermions	NNN [11]	–	NN [29]	–
HC Bosons	–	Contact [11]	Contact	?

V. DYNAMICS OF THE EXCITATIONS?

VI. CONCLUSIONS AND PERSPECTIVES

Ultracold atoms hopping in ladder geometries and subject to artificial magnetic fluxes are known to generate reach phase diagrams. For commensurate values of the ratio between the number of fluxes and the number of atoms, helical states with a net chiral current may appear. The simplest and most evident example of these helical states are the non-interacting Meissner phase for bosons and the helical state at flux $\chi = 2k_F$ for fermions. It is known, however, that additional pre-topological strogly correlated helical states originate for suitable values of the filling factor ν and suitable interactions [11, 12, 29, 51, 52, 55, 56, 61, 65].

In this work we argued that a two-leg ladder of hard-core bosons at $\nu = 1$ is characterized by one of these strongly-correlated helical states. We studied its signatures in terms of correlation functions, fluctuations, entanglement properties and dynamical evolution revise and complete... Our findings suggest that this state presents a large gap with respect to the pre-topological Laughlin-like states [11] and it is probably the easiest strongly-correlated helical state that can be realized and observed in current ultracold atom ladder experiments in synthetic dimension.

In particular, the strongly correlated $\nu = 1$ helical h–phase can be accessed in systems with contact interactions only, similarly to the bosonic Laughlin–like state at filling factor $\nu = 1/2$ [11]. With respect to this Laughlin–like state, the chiral current and gap signatures we observe are stronger. This is particularly relevant for experiments based on bosonic ladders like the Rb gases studied in the experiments in Refs. [22, 60].

Similarly to several quantum Hall states, strongly-correlated phases of bosons can be reached through interactions with a shorter range than their fermionic counterpart. This intuitively explains also why the gaps we detect for bosons at filling $\nu = 1$ are considerably larger than their fermionic counterpart at filling $\nu = 1/2$ [29]. In this respect, we find that bosonic systems are more suitable for the experimental characterization of these helical and strongly correlated phases of matter and the signatures of the $\nu = 1$ resonance are the strongest after the ones of the Meissner phase.

(In the following, if we wish, we can summarize more details... I would shorten howevere these following paragraphs)

We studied effects of commensurability between density and flux in a bosonic two-leg ladder with on-site and

rung interaction. The effective model is derived from assuming higher-order harmonics (i.e. $p = \pm 2$) in the bosonization identity. A second-order RG study reveals the existence of three distinct phases at commensurability $n = \chi/\pi$: (i) the trivial Luttinger liquid for large values of K_c and K_s, the h-dominated phase with pinned spin density field θ_s for any K_c and small K_s, and a hypothetical g-dominated phase with pinned charge density field θ_c which may appear with the addition of suitable longer-range interactions but it is suppressed by strong rung repulsions.

We then exploited the predicted phase diagram by DMRG simulations of hard core bosons and confirm the phase transition from Luttinger liquid to h-dominated phase at locked density-flux condition $\chi/\pi = n$. At the investigated interaction strengths, we could not confirm the existence of the g-dominated phase. For a follow-up study, the numerical results suggest to study better the higher order RG convergence of the g-dominated region in the predicted phase diagram. An experimental verification of the h-dominated phase is possible through a measurement of the chiral current j_c scaled versus the flux χ for a fixed system density.

ACKNOWLEDGMENTS

The authors wish to thank R. Citro and P. Schmoll for inspiring and enlightening discussions. A.H. is thankful for the financial support from the Max Planck Graduate Center. A.H. and M.R. acknowledge support from the Deutsche Forschungsgesellschaft (DFG) through the grant OSCAR 277810020 (RI 2345/2-1). M. B. is supported by the Villum Foundation (Research Grant No. 25310). Y. P. acknowledges financial support from the China Scholarships Council (grant No. 201906040093). The MPS simulations were run on the Mogon cluster of the Johannes Gutenberg-Universität (made available by the CSM and AHRP), with a code based on a flexible Abelian Symmetric Tensor Networks Library, developed in collaboration with the group of S. Montangero at the University of Ulm (now moved to Padua).

Appendix A: Bosonization of the model and derivation of the renormalization group equations

The field theoretical description of the hard–core boson ladder model has been developed based on bosonization techniques. In particular, the analysis of the behavior at the resonance $\chi = 2k_0$ requires a careful approach since there are two commonly used approximations that cannot be applied in this case. The first is related to the use of several harmonics to map the creation and annihilation operators of the lattice model into the low-energy description in the continuum: the resonance at $\chi = 2k_0$ appears evident only when taking into account higher harmonics, as in the case of the second-incommensurability effects studied in [18, 48, 49]. This is well-known in the analysis of the one-dimensional limits of fractional quantum Hall states (see, for example, [11, 12, 19, 29, 51, 52, 61]), where higher harmonics can also be interpreted as multi-particle interaction processes appearing in higher orders of perturbation theory [34, 47, 62]. The second important characteristics is that, for bosons at $\nu = 1$, there are two of these multi-particle processes that resonate and compose $\mathcal{O}_g$. These have exactly the same scaling behavior under the RG flow and hinder the possibility of adopting a simple semiclassical analysis. This situation is analogous to the case of fermionic ladder models at $\nu = 1/2$ [29] and requires a second-order renormalization group analysis to be examined. In this context the role of the h–term in (7) emerges and plays a crucial role.

In the following we will first present some of the details related to the derivation of the effective Hamiltonian (7), and then we will discuss the main steps to derive the RG equation in (9).

1. Bosonization of the hard-core boson model

We mentioned that the analysis of the resonant states appearing at specific values of the filling factor ν requires a bosonization of the lattice operators in terms of the series expansion of vertex operators (6) (see, for example, [14]). This series expansion rely on the non-universal coefficients β_p which are difficult to evaluate in non-integrable models. Instead of directly bosonize the hard-core bosons, in order to obtain an estimate of the most relevant of these non-universal parameter in our model, $\beta_{\pm 2}$, we will adopt a Jordan-Wigner transformation and use the standard bosonization of fermions instead.

To this purpose, we begin our analysis from the Hamiltonian:

$$\mathcal{H}_0 = -t \sum_{x,y} \left[b^\dagger_{x,y} b_{x+1,y} + \text{H.c.} \right] - \Omega \sum_x \left[\mathrm{e}^{i\chi x} b^\dagger_{x,\uparrow} b_{x,\downarrow} + \text{H.c.} \right] , \quad \text{(A1)}$$

This Hamiltonian is gauge–equivalent to (3), although this gauge choice breaks the translational invariance along x. In the Hamiltonian (A1), b and $b^\dagger$ are hard–core boson operators that can be related to one-dimensional fermionic operators c and $c^\dagger$ through the Jordan-Wigner transformation:

$$b_{x,y} = (-1)^{\sum_{j<x} c^\dagger_{j,y} c_{j,y}} c_{x,y} , \quad \text{(A2)}$$

$$b^\dagger_{x,y} = (-1)^{\sum_{j<x} c^\dagger_{j,y} c_{j,y}} c^\dagger_{x,y} . \quad \text{(A3)}$$

We define the total density of particles as $n_0 = N_{\text{tot}}/L$. In this mapping, the number of bosons and fermions match, such that $k_0 = \pi n_0/2$ becomes the Fermi momentum in the fermionic description. To bosonize the model

we adopt the standard bosonization of the fermionic operators (see, for example, [14, 23]):

$$c_{x,y} = \sqrt{\frac{k_0}{2\pi}} \left[\mathrm{e}^{-ik_0 x + i(\varphi_y(x)+\theta_y(x))} + \mathrm{e}^{ik_0 x + i(\varphi_y(x)-\theta_y(x))} \right], \tag{A4}$$

$$c^\dagger_{x,y} = \sqrt{\frac{k_0}{2\pi}} \left[\mathrm{e}^{ik_0 x - i(\varphi_y(x)+\theta_y(x))} + \mathrm{e}^{-ik_0 x - i(\varphi_y(x)-\theta_y(x))} \right], \tag{A5}$$

where θ_y and φ_y are two pairs of dual fields obeying commutation relations:

$$\left[\theta_{y'}(x'), \varphi_y(x)\right] = i\pi\delta_{yy'}\Theta(x'-x)\,. \tag{A6}$$

The density of each presudospin species can be approximated at first order in the harmonics expansion as:

$$n(x,y) \approx \frac{1}{\pi}\left[k_0 - \partial_x\theta_y(x)\right]\,. \tag{A7}$$

We use these equations to rewrite the Jordan-Wigner transformations in Eqs. (A2,A3). In particular, we symmetrize the JW string in the following way:

$$(-1)^{\sum_{j<x} c^\dagger_{j,y}c_{j,y}} = \frac{\mathrm{e}^{i\pi\sum_{j<x} c^\dagger_{j,y}c_{j,y}} + \mathrm{e}^{-i\pi\sum_{j<x} c^\dagger_{j,y}c_{j,y}}}{2} \to \frac{\mathrm{e}^{i(k_0x-\theta_y(x))} + \mathrm{e}^{-i(k_0x-\theta_y(x))}}{2}\,. \tag{A8}$$

From Eqs. (A4-A8) we obtain:

$$b_{x,y} \approx \sqrt{\frac{k_0}{2\pi}} \left[\mathrm{e}^{i\varphi_y(x)} + \frac{\mathrm{e}^{-2ik_0x}}{2}\mathrm{e}^{i(\varphi_y(x)+2\theta_y(x))} + \frac{\mathrm{e}^{2ik_0x}}{2}\mathrm{e}^{i(\varphi_y(x)-2\theta_y(x))} \right], \tag{A9}$$

$$b^\dagger_{x,y} \approx \sqrt{\frac{k_0}{2\pi}} \left[\mathrm{e}^{-i\varphi_y(x)} + \frac{\mathrm{e}^{2ik_0x}}{2}\mathrm{e}^{-i(\varphi_y(x)+2\theta_y(x))} + \frac{\mathrm{e}^{-2ik_0x}}{2}\mathrm{e}^{-i(\varphi_y(x)-2\theta_y(x))} \right], \tag{A10}$$

$$\tag{A11}$$

These equations correspond to the three most relevant terms in the expansion (6) and, from the mapping between hard–core bosons and fermions, we obtain $\beta_2 = \beta_{-2} = 1/2$, which is rigorous when considering separate chains, thus in the limit $\Omega \to 0$ and $V_\perp \to 0$. Due to the symmetry of the system, in the following we impose $\beta_2 = \beta_{-2}$. The estimate of the β parameters for general values of the interactions, the hopping Ω and the density of the system is an open problem. For several integrable models analytical solutions and numerical approximation are known (see, for example, [8, 57]).

Our model, in particular, can be mapped to a fermionic Hubbard model with interaction $V_\perp > 0$ in the limit $\Omega \to 0$ due to the previous Jordan-Wigner transformation (see also similar analysis in [19]). For the fermionic Hubbard model in the limit $V_\perp \to \infty$, the density modulations with momentum $2k_0$ are suppressed [23], such that we expect $\beta_{\pm 2}$ to be equally suppressed for large $V_\perp$. As we will discuss below, this has important implications in the determination of the phase diagram through the RG equations (9), however, since a precise estimate of β_2 for large interactions is difficult to derive and beyond the scope of our work, we decide to approximate it with the constant 1/2 irrespectively of the Hamiltonian parameters.

We observe that in the previous equations we did not introduce any Klein factor due to the bosonic nature of our model.

The interleg hopping and interactions can be analyzed by introducing the charge c and spin s sectors of the model through the unitary and canonical transformation:

$$\theta_c = \frac{\theta_\uparrow + \theta_\downarrow}{\sqrt{2}}\,, \quad \varphi_c = \frac{\varphi_\uparrow + \varphi_\downarrow}{\sqrt{2}}\,, \tag{A12}$$

$$\theta_s = \frac{\theta_\uparrow - \theta_\downarrow}{\sqrt{2}}\,, \quad \varphi_s = \frac{\varphi_\uparrow - \varphi_\downarrow}{\sqrt{2}}\,. \tag{A13}$$

The interleg hopping term reads:

$$\mathcal{H}_\Omega \to -\int \mathrm{d}x\, \Omega e^{i\chi x}\frac{k_0}{2\pi^2}\Big[\mathrm{e}^{-i\sqrt{2}\varphi_s} + \beta_2\mathrm{e}^{-i2k_0r}\mathrm{e}^{-i\sqrt{2}(\varphi_s+\theta_s+\theta_c)} + \beta_2\mathrm{e}^{-i2k_0r}\mathrm{e}^{-i\sqrt{2}(\varphi_s-\theta_s+\theta_c)} + \text{F.O.}\Big] + \text{H.c.} \tag{A14}$$

where we did not explicitly write additions fast oscillating term (F.O.) which are not resonant for $\chi = 2k_0$. The terms oscillating as e^{i2k_0r} in the parenthesis of Eq. (A14) are resonant for $\nu = 1$ and yield the g–term of the interactions in Eq. (7) and the initial value of the coupling constant g in the RG flow in Eq. (8).

Concerning the h–term in Eq. (7), this interaction is dictated by the $2k_0x$ harmonics of the bosonic operators; in particular, Eq. (A7) must be supplemented by additional higher-order oscillating terms [14]. The first of these terms can be estimated from a point-splitting procedure of the operators (A9,A10), by evaluating $b^\dagger\left(x-\delta x/2\right)b(x+\delta x/2)$ with $\delta x = k_0^{-1}$. In this

way, we obtain the estimate:

$$\delta n(x,y) \approx \frac{\beta_2}{\pi}\left[k_0 - \partial_x\theta_y(x)\right]\sin\left(2k_0x - 2\theta_y(x)\right)\,. \tag{A15}$$

This implies that the interleg rung interaction becomes:

$$\mathcal{H}_\perp \to \int \mathrm{d}x\,\frac{V_\perp}{2\pi^2}\left[(\partial_x\theta_c)^2 - (\partial_x\theta_s)^2\right] + \int \mathrm{d}x\,V_\perp\frac{\beta_2^2k_0^2}{2\pi^2}\cos\left(2\sqrt{2}\theta_s(x)\right) \tag{A16}$$

where we neglected fast-oscillating and boundary terms. The interaction (A16) is responsible for the initial values of the RG flow of both the Luttinger parameters and the coupling constant h in Eqs. (8) and (10).

2. Renormalization group equations

The second-order renormalization group analysis of the Hamiltonian (7) follows the analogous fermionic case at filling $\nu = 1/2$ [29]. We apply, in particular, the Wilsonian RG in momentum space at second order.

The crucial point is that we consider the interaction terms h and g in Eq. (7) as a perturbation of the gapless Luttinger liquid. Therefore, we expect our results to be valid when the bare values of g and h are much smaller than 1. In particular, by imposing $\Omega = 0.05$ and $N/L = 48/64$ as in the numerical simulations, we obtain that the general features of the phase diagram defined by the second-order equations (9) is stable until $V_\perp < 6t$. Beyond this threshold non-physical features emerge which are not compatible with the MPS simulations, thus indicating that a second-order perturbation approach fails beyond this limit.

We summarize in the following the main steps for the derivation of Eqs (9).

For each of the bosonic fields we distinguish fast and slow modes, separated by an effective cutoff in momentum space that we label $\tilde{\Lambda}$. Furthermore, we introduce an ultraviolet momentum cutoff $\Lambda > \tilde{\Lambda}$. The fast oscillating modes are characterized by $\tilde{\Lambda} < k < \Lambda$ and we are interested in the limit $\Lambda/\tilde{\Lambda} = 1 + dl$, with dl infinitesimal. The bosonic fields can thus be decomposed into:

$$\varphi_a(x,t) = \varphi_{\mathsf{s},a}(x,t) + \varphi_{\mathsf{f},a}(x,t)\,, \tag{A17}$$
$$\theta_a(x,t) = \theta_{\mathsf{s},a}(x,t) + \theta_{\mathsf{f},a}(x,t)\,. \tag{A18}$$

We separate the action of the model for $\chi = 2k_0$ in Euclidean space into a Gaussian part and an interacting part, and we consider the latter as a perturbation:

$$S = \frac{1}{2\pi}\int \mathrm{d}^2x\left[\sum_{a=s,c}\frac{K_a}{v_a}(\partial_t\varphi_a)^2 + K_av_a(\partial_x\varphi_a)^2\right] + \int \mathrm{d}^2x\left[g\mathcal{O}_g + h\cos\left(2\sqrt{2}\theta_s(x)\right)\right]. \tag{A19}$$

Our aim is to obtain an effective action for the slow modes only by integrating out the fast degrees of freedom:

$$\begin{aligned} S_{\mathrm{eff}}(\tilde{\Lambda}) &= S_0(\varphi_{\mathsf{s}}) - \ln\left\langle e^{-S_I(\varphi_{\mathsf{s}}+\varphi_{\mathsf{f}})}\right\rangle_{\mathsf{f}} \\ &\approx S_0(\varphi_{\mathsf{s}}) + \underbrace{\langle S_I(\varphi_{\mathsf{s}}+\varphi_{\mathsf{f}})\rangle_{\mathsf{f}}}_{\mathcal{A}} \\ &- \frac{1}{2}\left(\underbrace{\left\langle S_I^2(\varphi_{\mathsf{s}}+\varphi_{\mathsf{f}})\right\rangle_{\mathsf{f}}}_{\mathcal{B}} - \underbrace{\langle S_I(\varphi_{\mathsf{s}}+\varphi_{\mathsf{f}})\rangle_{\mathsf{f}}^2}_{\mathcal{A}^2}\right) + \dots\,, \end{aligned} \tag{A20}$$

where we identified the effective action at the second order of perturbation theory. The Gaussian correlation functions for the bosonic fields can be approximated as:

$$\left\langle\varphi_{\mathsf{f},a}^2(x)\right\rangle_{\mathsf{f}} = \int_{\tilde{\Lambda}<k<\Lambda}\frac{d^2k}{4\pi}\frac{1}{K_ak^2} = \frac{1}{2K_a}\ln\frac{\Lambda}{\tilde{\Lambda}}\,, \tag{A21}$$

$$\langle\varphi_{\mathsf{f},a}(x_1,t_1)\varphi_{\mathsf{f},a}(x_2,t_2)\rangle_{\mathsf{f}} = \int_{\tilde{\Lambda}}^{\Lambda}\frac{dk}{2}\frac{J_0(kr)}{K_ak} \approx \frac{C(r_a)}{2K_a}\ln\frac{\Lambda}{\tilde{\Lambda}}\,, \tag{A22}$$

$$\left\langle\theta_{\mathsf{f},a}^2(x)\right\rangle_{\mathsf{f}} = \frac{K_a}{2}\ln\frac{\Lambda}{\tilde{\Lambda}}\,, \tag{A23}$$

$$\langle\theta_{\mathsf{f},a}(x_1,t_1)\theta_{\mathsf{f},a}(x_2,t_2)\rangle_{\mathsf{f}} \approx \frac{C(r_a)K_a}{2}\ln\frac{\Lambda}{\tilde{\Lambda}}\,. \tag{A24}$$

Here the logarithm captures the scaling behavior, and $C(r_a)$ is a function of $r_a = \sqrt{u_a^2(t_1-t_2)^2 + (x_1-x_2)^2}$. In the following we will consider $C(r)$ to be suitably short-ranged; in the case of a sharp cutoff, $C(r) \approx J_0(\Lambda r)$ and this assumption is not satisfactorily fulfilled, but $C(r)$ can be made sufficiently short-ranged with more refined cutoffs [37].

The terms in $\mathcal{A}$ return the usual first–order dependence of the RG equations on the scaling dimensions (thus the first terms in the $\mathrm{d}g/\mathrm{d}l$ and $\mathrm{d}h/\mathrm{d}l$ in Eq. (9)). We focus on the terms appearing in $\mathcal{B}$. There are four terms originating from $\mathcal{O}_g$ at second-order: two of them contribute to the quadratic part of the Hamiltonian and determine the g^2 correction to the Luttinger parameters; one of them is proportional to the h–term, and determines the crucial dependence of $\mathrm{d}h/\mathrm{d}l$ on g^2; the last term is instead less relevant than the h and g interactions and we will neglect it. Concerning the terms originating from h, also in this case we have a contribution proportional to h^2 that affects the flow of the Luttinger parameters and additional interactions which are less relevant that the term in S_I and can be discarded. Finally there is a contribution to the coupling constant g obtained from the product between the g and h operators.

Let us consider first the terms generating corrections to the Gaussian part of the action. They read:

$$
\begin{aligned}
&-\frac{1}{2}\int \mathrm{d}^2x_1\mathrm{d}^2x_2 \sum_{\mu,\nu=\pm1} g^2 \left\langle \mathrm{e}^{i\nu\sqrt{2}(\varphi_s+\mu\theta_s+\theta_c)(x_1)}\mathrm{e}^{-i\nu\sqrt{2}(\varphi_s+\mu\theta_s+\theta_c)(x_2)}\right\rangle_{\mathsf{f}} + \frac{h^2}{4}\sum_{\nu=\pm1}\left\langle \mathrm{e}^{i\nu 2\sqrt{2}\theta_s(x_1)}\mathrm{e}^{-i\nu 2\sqrt{2}\theta_s(x_2)}\right\rangle_{\mathsf{f}} \\
&= \frac{g^2}{2}\int \mathrm{d}^2x_1\mathrm{d}^2x_2 \sum_{\mu,\nu=\pm1} e^{i\nu\sqrt{2}[\varphi_{\mathsf{s},s}(x_1)+\mu\theta_{\mathsf{s},s}(x_1)+\theta_{\mathsf{s},c}(x_1)-\varphi_{\mathsf{s},s}(x_2)-\mu\theta_{\mathsf{s},s}(x_2)-\theta_{\mathsf{s},c}(x_2)]}\left(\frac{\Lambda}{\tilde{\Lambda}}\right)^{\left[(C(r_s)-1)\left(K_s^{-1}+K_s\right)+(C(r_c)-1)K_c\right]} \\
&\qquad -\frac{h^2}{8}\int \mathrm{d}^2x_1\mathrm{d}^2x_2 \sum_{\nu=\pm1} e^{i2\sqrt{2}\nu(\theta_{\mathsf{s},s}(x_1)-\theta_{\mathsf{s},s}(x_2))}\left(\frac{\Lambda}{\tilde{\Lambda}}\right)^{4[C(r_s)-1]K_s} . \qquad \text{(A25)}
\end{aligned}
$$

Since $\Lambda/\tilde{\Lambda} = 1 + \mathrm{d}l$, in the previous equation the first-order terms in $\mathrm{d}l$, which determine the RG equations, are the sum of contributions proportional to C and contributions independent of C. Only the former enter in the renormalization of the Luttinger parameters because the latter are canceled by subtracting the analogous contributions from $\mathcal{A}^2$. Hence we focus only on the terms proportional to $C\mathrm{d}l$. In the previous expression, we distinguished with the labels r_s and r_c the relative space time coordinates between X_1 and x_2 calculated with u_s and u_c respectively.

We consider that C is a short range function, such that we can split the integrals into the integral of the center of mass coordinates $x = (x_1 + x_2)/2$, and the relative coordinates. The correlation function is non-negligible only in a neighborhood of size α around $r = 0$, where α is, in general, a non-universal constant of the order of the lattice spacing a. The integral over the relative coordinates, therefore, returns a constant of order $\alpha^2/u_{c,s}$ and constrains x_1 and x_2 to be within a range α from each other. Hence, integrating over the relative coordinate we can approximate the terms proportional to $C\mathrm{d}l$ as:

$$
\begin{aligned}
&\frac{g^2\alpha^2\mathrm{d}l}{u_s}\int \mathrm{d}^2x \sum_{\mu=\pm1}\left(K_s^{-1}+K_s\right)\cos\left[\alpha\sqrt{2}\partial_{r_s}\left(\varphi_s+\mu\theta_s+\theta_c\right)\right] + \frac{g^2\alpha^2\mathrm{d}l}{u_c}\int \mathrm{d}^2x \sum_{\mu=\pm1} K_c\cos\left[\alpha\sqrt{2}\partial_{r_c}\left(\varphi_s+\mu\theta_s+\theta_c\right)\right] \\
&\qquad -\frac{h^2\alpha^2\mathrm{d}l}{4u_s}\int \mathrm{d}^2x\, 4K_s\cos\left[\alpha 2\sqrt{2}\partial_{r_s}\theta_s\right] \\
&\approx -\frac{2\alpha^4g^2\mathrm{d}l}{u_s}\left(K_s^{-1}+K_s\right)\int \mathrm{d}^2x\left[\left(\partial_x\varphi_s\right)^2+\left(\partial_x\theta_s\right)^2+\left(\partial_x\theta_c\right)^2+\frac{\left(\partial_t\varphi_s\right)^2+\left(\partial_t\theta_s\right)^2+\left(\partial_t\theta_c\right)^2}{u_s^2}+2\partial_x\varphi_s\partial_x\theta_c+2\frac{\partial_t\varphi_s\partial_t\theta_c}{u_s^2}\right] \\
&\qquad -\frac{2\alpha^4g^2\mathrm{d}l}{u_c}K_c\int \mathrm{d}^2x\left[\left(\partial_x\varphi_s\right)^2+\left(\partial_x\theta_s\right)^2+\left(\partial_x\theta_c\right)^2+\frac{\left(\partial_t\varphi_s\right)^2+\left(\partial_t\theta_s\right)^2+\left(\partial_t\theta_c\right)^2}{u_c^2}+2\partial_x\varphi_s\partial_x\theta_c+2\frac{\partial_t\varphi_s\partial_t\theta_c}{u_0^2}\right] \\
&\qquad +\frac{4h^2\alpha^4K_s\mathrm{d}l}{u_s}\int \mathrm{d}^2x\left[\left(\partial_x\theta_s\right)^2+\frac{\left(\partial_t\theta_s\right)^2}{u_s^2}\right] \qquad \text{(A26)}
\end{aligned}
$$

where we dropped the labels s of the slow modes and the explicit coordinate dependence. We observe that in this approximation there appear two terms mixing φ_s and θ_c, thus the spin and change sectors. These terms break the possibility of rigorously diagonalizing the system into these separate sectors and would require to introduce a unitary matrix, dependent on l, to diagonalize the Gaussian part of the action at each scale. For the sake of simplicity, however, we neglect this mixing and we consider only the standard correction to the Luttinger parameters K_s and K_c. To finally evaluate the $\mathrm{d}l$ corrections to the Gaussian action we recall the duality relations in Euclidean coordinates:

$$
\partial_t\theta_j = iu_jK_j\partial_x\varphi_j\,, \quad \partial_t\varphi_j = i\frac{u_j}{K_j}\partial_x\theta_j\,. \qquad \text{(A27)}
$$

Based on the previous relations we find the renormalized values of the Luttinger parameters:

$$
K_c' \approx K_c + 4\pi\alpha^4g^2\mathrm{d}l\left[\frac{K_c}{u_c^2}+\left(K_s+K_s^{-1}\right)\frac{u_s^2+u_c^2}{2u_cu_s^3}\right]K_c^2\,, \qquad \text{(A28)}
$$

$$
K_s' \approx K_s - \frac{8\pi\alpha^4h^2K_s^3\mathrm{d}l}{u_s^2} - 4\pi\alpha^4g^2\mathrm{d}l\left(1-K_s^2\right)\left[\frac{u_c^2+u_s^2}{2u_su_c^3}K_c+\frac{K_s+K_s^{-1}}{u_s^2}\right]. \qquad \text{(A29)}
$$

These renormalized values determine the RG equations for the Luttinger parameters in Eq. (9) (where we set $\alpha = 1$).

To conclude the derivation of the second-order equations concerning the h and g coupling constants, we derive the contribution proportional to $g^2\mathrm{d}l$ to the renormalized coupling constant h, and the contribution proportional to $gh\mathrm{d}l$

to the renormalized coupling constant g. These terms are obtained from the following parts of $-\mathcal{B}/2$:

$$
\begin{aligned}
&-\frac{1}{2}\int \mathrm{d}^2x_1\mathrm{d}^2x_2 \sum_{\mu,\nu=\pm1} g^2 \left\langle \mathrm{e}^{i\nu\sqrt{2}(\varphi_s+\mu\theta_s+\theta_c)(x_1)}\mathrm{e}^{-i\nu\sqrt{2}(\varphi_s-\mu\theta_s+\theta_c)(x_2)}\right\rangle_{\mathsf{f}} \\
&\qquad\qquad + \frac{gh}{4}\sum_{\mu,\nu=\pm1}\left\langle \mathrm{e}^{i\nu\mu 2\sqrt{2}\theta_s(x_1)}\mathrm{e}^{-i\nu\sqrt{2}(\varphi_s-\mu\theta_s+\theta_c)(x_2)} + (x_1\leftrightarrow x_2)\right\rangle_{\mathsf{f}} \\
&= \frac{g^2}{2}\int \mathrm{d}^2x_1\mathrm{d}^2x_2 \sum_{\mu,\nu=\pm1} e^{i\nu\sqrt{2}[\varphi_{\mathsf{s},s}(x_1)+\mu\theta_{\mathsf{s},s}(x_1)+\theta_{\mathsf{s},c}(x_1)-\varphi_{\mathsf{s},s}(x_2)+\mu\theta_{\mathsf{s},s}(x_2)-\theta_{\mathsf{s},c}(x_2)]}\left(\frac{\Lambda}{\tilde{\Lambda}}\right)^{(C(r_s)-1)\left(K_s^{-1}-K_s\right)+(C(r_c)-1)K_c} \\
&\quad -\frac{gh}{4}\int \mathrm{d}^2x_1\mathrm{d}^2x_2 \sum_{\nu,\mu=\pm1}\left[\mathrm{e}^{-i\nu\sqrt{2}(\varphi_{\mathsf{s},s}(x_2)-\mu\theta_{\mathsf{s},s}(x_2)+2\mu\theta_{\mathsf{s},s}(x_1)+\theta_{\mathsf{s},c}(x_2))}+(x_1\leftrightarrow x_2)\right]\left(\frac{\Lambda}{\tilde{\Lambda}}\right)^{\left[2K_sC(r_s)-\frac{1}{2K_s}-\frac{5K_s}{2}-\frac{K_c}{2}\right]}.
\end{aligned}
\tag{A30}
$$

Also in this case we are interested only in the terms proportional to $C(r_a)\mathrm{d}l$; furthermore, since we are searching for the most relevant contributions only, we approximate $C(r_a)\approx\gamma_a\delta^{(2)}(x_1-x_2)$ where γ_a is a non-universal constant of order a^2/u_a. The resulting terms reads:

$$
2g^2\mathrm{d}l\left(\gamma_sK_s^{-1}-\gamma_sK_s+\gamma_cK_c\right)\int \mathrm{d}^2x\,\cos\left(2\sqrt{2}\theta_s\right) - ghK_s\gamma_s\mathrm{d}l\int \mathrm{d}^2x\,\mathcal{O}_g\,. \tag{A31}
$$

These terms determine the second order contributions to the RG equations of the g and h coupling constants in Eq. (9) (where we set $\gamma_a=1/u_a$). In our numerical solutions of the RG equations (9) we checked that small variations of the non-universal parameters γ and α around 1 do not qualitatively affect the phase diagram in Fig. 2.

3. Further details about the correlation functions

The calculation of the correlation functions of the θ and φ fields for finite systems depends on the boundary conditions. In principle, we should separately consider the charge and spin sectors. For the charge sector indeed, no particle can tunnel in or out of the system from the boundaries, and the charge current must exactly vanish at the boundaries. Therefore $\partial_x\varphi_c=0$ for both $x=0$ and $x=L$. For the spin sector, instead, the total spin density is not conserved and, although the chiral current must vanish in average at the boundaries, the previous Neumann boundary conditions for φ_s is in principle too restrictive, and one should consider more general kinds of boundary conditions [6, 10, 39, 44]. We expect, however, the deviation from the Neumann boundary conditions to be small (proportional to Ω/t), and, also for the spin case, we will consider $\partial_x\varphi_s=0$ at the edges. Based on the construction in [14] (see also [39, 44]), we can define the charge and spin fields (at time $t=0$) in the form:

$$
\sqrt{K_a}\varphi_a = \varphi_0 + \sum_k{}' \frac{1}{\sqrt{2|k|}}\left[e^{i\frac{k\pi x}{2L}}b_{a,k}+e^{-i\frac{k\pi x}{2L}}b_{a,k}^\dagger\right], \tag{A32}
$$

$$
\frac{\theta_a}{\sqrt{K_a}} = \theta_0 + \sum_k{}' \frac{\mathrm{sign}k}{\sqrt{2|k|}}\left[e^{i\frac{k\pi x}{2L}}b_{a,k}+e^{-i\frac{k\pi x}{2L}}b_{a,k}^\dagger\right]; \tag{A33}
$$

where $\sum'$ labels the sum over the even integers k, with $k\neq0$ from $-\infty$ to $+\infty$. Here $b_{a,k}$ labels two sets of bosonic annihilation and creation operators related to the spin and charge sectors respectively. In order to fulfill the Neumann oundary conditions, we must impose:

$$
b_{a,k} = b_{a,-k}\,. \tag{A34}
$$

From the previous relations we derive:

$$
\langle\theta_a(x)\theta_a(x')\rangle = -\frac{K_a}{2}\ln\left[\frac{d(x-x'|2L)}{d(x+x'|2L)}\right], \tag{A35}
$$

$$
\langle\varphi_a(x)\varphi_a(x')\rangle = -\frac{1}{2K_a}\ln\left[d(x-x'|2L)d(x+x'|2L)\right], \tag{A36}
$$

Considering the case $x'\to0$, and neglecting functions of x' only, we obtain the behavior (15) for the spin and charge fluctuations. Given the deviation from the Neumann boundary conditions of the spin sector, however, we must account for an additional weak space dependence represented by the function $f_s(x)$.

(On a very mathematical perspective, one should impose generalized boundary conditions $\partial_x\varphi_s(x=0)=$

$\alpha\varphi_s(x=0)$ in the spin sector. α is a parameter related to the scattering matrix of the edge. Everything can be solved as a function of α following Mintchev's works, but α should be fitted. This would probably help improving our estimates of K_s but, despite the fact that I think it would be very cool, I do not want to delay this work so much.)

Old stuff to be erased below

Analytic expressions for correlation functions of the bosonic fields are well known [14]. Their expressions are obtained by assuming the momentum fluctuations to be zero at the boundary of the chain (i.e. there is no persistent current for Dirichlet boundary conditions), which allows to "unfold" the fields in such a way that right movers are identical to space-inverted left movers. For the following analysis, it is more convenient to write the correlations in integrated form, such that we find logarithmic decays of the ratio and product of two chord distances

$$\langle\theta_i(x)\theta_i(x')\rangle = -\frac{K_i}{2}\ln\left[\frac{d(x-x'|2L)}{d(x+x'|2L)}\right], \tag{A37}$$

$$\langle\varphi_i(x)\varphi_i(x')\rangle = -\frac{1}{2K_i}\ln\left[d(x-x'|2L)d(x+x'|2L)\right].$$

(Michele: I have some issues with these equations. First, for $x'\to 0$, the $\theta_c\theta_c$ correlation must be compatible with (14) and (15). This requires to change $d(x|L)$ into $d(2x|2L)$ in Eq. (15). Second, we have different boundary conditions in the charge and spin sectors. The charge sector has the currents that die at the boundaries due to the particle conservation, whereas the spin sector does not have this constraint. This leads, in principle, to different correlations in the two sectors. In particular I would say that these equations are ok for the charge sector, but considerable deviations for both the correlations and the fluctuations may be expected in the spin sector.)

In Eq. (A35) we present indefinite integrals and a general solution may contain additional constants and linear terms $\propto x, x', xx'$. The constants can be trivially neglected as they do not alter the decay of correlation functions. However, linear terms may arise as a consequence from broken symmetries due to interactions or superconducting terms [52]. Note that such terms depend on the real space distance rather than the chord distance.

---

[1] M. Aidelsburger, M. Atala, M. Lohse, J. T. Barreiro, B. Paredes, and I. Bloch. Realization of the hofstadter hamiltonian with ultracold atoms in optical lattices. *Phys. Rev. Lett.*, 111:185301, Oct 2013.

[2] Monika Aidelsburger, Michael Lohse, Christian Schweizer, Marcos Atala, Julio T Barreiro, Sylvain Nascimbène, NR Cooper, Immanuel Bloch, and Nathan Goldman. Measuring the chern number of hofstadter bands with ultracold bosonic atoms. *Nature Physics*, 11(2):162–166, 2015.

[3] Marcos Atala, Monika Aidelsburger, Michael Lohse, Julio T Barreiro, Belén Paredes, and Immanuel Bloch. Observation of chiral currents with ultracold atoms in bosonic ladders. *Nature Physics*, 10(8):588–593, 2014.

[4] S Barbarino, D Rossini, M Rizzi, R Fazio, GE Santoro, and M Dalmonte. Topological devil's staircase in atomic two-leg ladders. *New Journal of Physics*, 21(4):043048, 2019.

[5] Simone Barbarino, Marcello Dalmonte, Rosario Fazio, and Giuseppe E Santoro. Topological phases in frustrated synthetic ladders with an odd number of legs. *Physical Review A*, 97(1):013634, 2018.

[6] B Bellazzini, M Burrello, M Mintchev, and P Sorba. Quantum field theory on star graphs. *Proc. Symp. Pure Math.*, 77:639, 2008.

[7] O Boada, A Celi, JI Latorre, and M Lewenstein. Quantum simulation of an extra dimension. *Physical review letters*, 108(13):133001, 2012.

[8] Pierre Bouillot, Corinna Kollath, Andreas M. Läuchli, Mikhail Zvonarev, Benedikt Thielemann, Christian Rüegg, Edmond Orignac, Roberta Citro, Martin Klanjšek, Claude Berthier, Mladen Horvatić, and Thierry Giamarchi. Statics and dynamics of weakly coupled antiferromagnetic spin-$\frac{1}{2}$ ladders in a magnetic field. *Phys. Rev. B*, 83:054407, Feb 2011.

[9] Maximilian Buser, Fabian Heidrich-Meisner, and Ulrich Schollwöck. Finite-temperature properties of interacting bosons on a two-leg flux ladder. *Phys. Rev. A*, 99:053601, May 2019.

[10] Pasquale Calabrese, Mihail Mintchev, and Ettore Vicari. Entanglement entropy of quantum wire junctions. *Journal of Physics A: Mathematical and Theoretical*, 45(10):105206, 2012.

[11] Marcello Calvanese Strinati, Eyal Cornfeld, Davide Rossini, Simone Barbarino, Marcello Dalmonte, Rosario Fazio, Eran Sela, and Leonardo Mazza. Laughlin-like states in bosonic and fermionic atomic synthetic ladders. *Phys. Rev. X*, 7:021033, Jun 2017.

[12] Marcello Calvanese Strinati, Sharmistha Sahoo, Kirill Shtengel, and Eran Sela. Pretopological fractional excitations in the two-leg flux ladder. *Phys. Rev. B*, 99:245101, Jun 2019.

[13] Sam T Carr, Boris N Narozhny, and Alexander A Nersesyan. Spinless fermionic ladders in a magnetic field: phase diagram. *Physical Review B*, 73(19):195114, 2006.

[14] M A Cazalilla. Bosonizing one-dimensional cold atomic

gases. *Journal of Physics B: Atomic, Molecular and Optical Physics*, 37(7):S1–S47, mar 2004.

[15] A. Celi, P. Massignan, J. Ruseckas, N. Goldman, I. B. Spielman, G. Juzeliūnas, and M. Lewenstein. Synthetic gauge fields in synthetic dimensions. *Phys. Rev. Lett.*, 112:043001, Jan 2014.

[16] Jian-Dong Chen, Hong-Hao Tu, Ying-Hai Wu, and Zhi-Fang Xu. Quantum phases of two-component bosons on the harper-hofstadter ladder. *arXiv preprint arXiv:1912.03105*, 2019.

[17] Cheng Chin, Rudolf Grimm, Paul Julienne, and Eite Tiesinga. Feshbach resonances in ultracold gases. *Rev. Mod. Phys.*, 82:1225–1286, Apr 2010.

[18] R. Citro, S. De Palo, M. Di Dio, and E. Orignac. Quantum phase transitions of a two-leg bosonic ladder in an artificial gauge field. *Phys. Rev. B*, 97:174523, May 2018.

[19] Eyal Cornfeld and Eran Sela. Chiral currents in one-dimensional fractional quantum hall states. *Phys. Rev. B*, 92:115446, Sep 2015.

[20] Fran çois Crépin, Nicolas Laflorencie, Guillaume Roux, and Pascal Simon. Phase diagram of hard-core bosons on clean and disordered two-leg ladders: Mott insulator–luttinger liquid–bose glass. *Phys. Rev. B*, 84:054517, Aug 2011.

[21] GI Dzhaparidze and AA Nersesyan. Magnetic-field phase transition in a one-dimensional system of electrons with attraction. *JETP Lett*, 27(6), 1978.

[22] Dina Genkina, Lauren M Aycock, Hsin-I Lu, Mingwu Lu, Alina M Pineiro, and IB Spielman. Imaging topology of hofstadter ribbons. *New Journal of Physics*, 21(5):053021, 2019.

[23] T. Giamarchi. *Quantum Physics in One Dimension*. International Series of Monographs on Physics. Clarendon Press, 2003.

[24] A.O. Gogolin, A.A. Nersesyan, and A.M. Tsvelik. *Bosonization and Strongly Correlated Systems*. Cambridge University Press, 2004.

[25] S. Greschner, M. Piraud, F. Heidrich-Meisner, I. P. McCulloch, U. Schollwöck, and T. Vekua. Spontaneous increase of magnetic flux and chiral-current reversal in bosonic ladders: Swimming against the tide. *Phys. Rev. Lett.*, 115:190402, Nov 2015.

[26] S. Greschner, M. Piraud, F. Heidrich-Meisner, I. P. McCulloch, U. Schollwöck, and T. Vekua. Symmetry-broken states in a system of interacting bosons on a two-leg ladder with a uniform abelian gauge field. *Phys. Rev. A*, 94:063628, Dec 2016.

[27] S. Greschner and T. Vekua. Vortex-hole duality: A unified picture of weak- and strong-coupling regimes of bosonic ladders with flux. *Phys. Rev. Lett.*, 119:073401, Aug 2017.

[28] Sebastian Greschner, Michele Filippone, and Thierry Giamarchi. Universal hall response in interacting quantum systems. *Physical review letters*, 122(8):083402, 2019.

[29] Andreas Haller, Matteo Rizzi, and Michele Burrello. The resonant state at filling factor $\nu = 1/2$ in chiral fermionic ladders. *New Journal of Physics*, 20(5):053007, may 2018.

[30] Jeong Ho Han, Jin Hyoun Kang, and Y. Shin. Band gap closing in a synthetic hall tube of neutral fermions. *Phys. Rev. Lett.*, 122:065303, Feb 2019.

[31] Dario Hügel and Belén Paredes. Chiral ladders and the edges of quantum hall insulators. *Physical Review A*, 89(2):023619, 2014.

[32] Dario Hügel, Hugo UR Strand, Philipp Werner, and Lode Pollet. Anisotropic harper-hofstadter-mott model: Competition between condensation and magnetic fields. *Physical Review B*, 96(5):054431, 2017.

[33] J. Jünemann, A. Piga, S.-J. Ran, M. Lewenstein, M. Rizzi, and A. Bermudez. Exploring interacting topological insulators with ultracold atoms: The synthetic creutz-hubbard model. *Phys. Rev. X*, 7:031057, Sep 2017.

[34] C. L. Kane, Ranjan Mukhopadhyay, and T. C. Lubensky. Fractional quantum hall effect in an array of quantum wires. *Phys. Rev. Lett.*, 88:036401, Jan 2002.

[35] Jin Hyoun Kang, Jeong Ho Han, and Yong-il Shin. Realization of a cross-linked chiral ladder with neutral fermions in a 1d optical lattice by orbital-momentum coupling. *Physical review letters*, 121(15):150403, 2018.

[36] Ahmet Keleş and M. Ö. Oktel. Mott transition in a two-leg bose-hubbard ladder under an artificial magnetic field. *Phys. Rev. A*, 91:013629, Jan 2015.

[37] John B. Kogut. An introduction to lattice gauge theory and spin systems. *Rev. Mod. Phys.*, 51:659–713, Oct 1979.

[38] Filip Kozarski, Dario Hügel, and Lode Pollet. Quasi-one-dimensional hall physics in the harper–hofstadter–mott model. *New Journal of Physics*, 20(4):043001, 2018.

[39] Antonio Liguori and Mihail Mintchev. Quantum field theory, bosonization and duality on the half line. *Nuclear Physics B*, 522(1-2):345–372, 1998.

[40] L. F. Livi, G. Cappellini, M. Diem, L. Franchi, C. Clivati, M. Frittelli, F. Levi, D. Calonico, J. Catani, M. Inguscio, and L. Fallani. Synthetic dimensions and spin-orbit coupling with an optical clock transition. *Phys. Rev. Lett.*, 117:220401, Nov 2016.

[41] Marco Mancini, Guido Pagano, Giacomo Cappellini, Lorenzo Livi, Marie Rider, Jacopo Catani, Carlo Sias, Peter Zoller, Massimo Inguscio, Marcello Dalmonte, et al. Observation of chiral edge states with neutral fermions in synthetic hall ribbons. *Science*, 349(6255):1510–1513, 2015.

[42] A. Marte, T. Volz, J. Schuster, S. Dürr, G. Rempe, E. G. M. van Kempen, and B. J. Verhaar. Feshbach resonances in rubidium 87: Precision measurement and analysis. *Phys. Rev. Lett.*, 89:283202, Dec 2002.

[43] Leonardo Mazza, Monika Aidelsburger, Hong-Hao Tu, Nathan Goldman, and Michele Burrello. Methods for detecting charge fractionalization and winding numbers in an interacting fermionic ladder. *New journal of physics*, 17(10):105001, 2015.

[44] Mihail Mintchev and Paul Sorba. Bosonization and vertex algebras with defects. In *Annales Henri Poincare*, volume 7, pages 1375–1393. Springer, 2006.

[45] Hirokazu Miyake, Georgios A. Siviloglou, Colin J. Kennedy, William Cody Burton, and Wolfgang Ketterle. Realizing the harper hamiltonian with laser-assisted tunneling in optical lattices. *Phys. Rev. Lett.*, 111:185302, Oct 2013.

[46] Ritu Nehra, Devendra Singh Bhakuni, Suhas Gangadharaiah, and Auditya Sharma. Many-body entanglement in a topological chiral ladder. *Physical Review B*, 98(4):045120, 2018.

[47] Yuval Oreg, Eran Sela, and Ady Stern. Fractional helical liquids in quantum wires. *Phys. Rev. B*, 89:115402, Mar 2014.

[48] E. Orignac, R. Citro, M. Di Dio, and S. De Palo. Vortex

lattice melting in a boson ladder in an artificial gauge field. *Phys. Rev. B*, 96:014518, Jul 2017.

[49] E Orignac, R Citro, M Di Dio, S De Palo, and M-L Chiofalo. Incommensurate phases of a bosonic two-leg ladder under a flux. *New Journal of Physics*, 18(5):055017, may 2016.

[50] E. Orignac and T. Giamarchi. Meissner effect in a bosonic ladder. *Phys. Rev. B*, 64:144515, Sep 2001.

[51] Alexandru Petrescu and Karyn Le Hur. Chiral mott insulators, meissner effect, and laughlin states in quantum ladders. *Phys. Rev. B*, 91:054520, Feb 2015.

[52] Alexandru Petrescu, Marie Piraud, Guillaume Roux, I. P. McCulloch, and Karyn Le Hur. Precursor of the laughlin state of hard-core bosons on a two-leg ladder. *Phys. Rev. B*, 96:014524, Jul 2017.

[53] M. Piraud, F. Heidrich-Meisner, I. P. McCulloch, S. Greschner, T. Vekua, and U. Schollwöck. Vortex and meissner phases of strongly interacting bosons on a two-leg ladder. *Phys. Rev. B*, 91:140406, Apr 2015.

[54] VL Pokrovsky and AL Talapov. Ground state, spectrum, and phase diagram of two-dimensional incommensurate crystals. *Physical Review Letters*, 42(1):65, 1979.

[55] Paolo Rosson, Michael Lubasch, Martin Kiffner, and Dieter Jaksch. Bosonic fractional quantum hall states on a finite cylinder. *Physical Review A*, 99(3):033603, 2019.

[56] Raul A Santos and Benjamin Béri. Fractional topological insulator precursors in spin-orbit fermion ladders. *Physical Review B*, 100(23):235122, 2019.

[57] Aditya Shashi, Miłosz Panfil, Jean-Sébastien Caux, and Adilet Imambekov. Exact prefactors in static and dynamic correlation functions of one-dimensional quantum integrable models: Applications to the calogero-sutherland, lieb-liniger, and xxz models. *Phys. Rev. B*, 85:155136, Apr 2012.

[58] H. Francis Song, Stephan Rachel, Christian Flindt, Israel Klich, Nicolas Laflorencie, and Karyn Le Hur. Bipartite fluctuations as a probe of many-body entanglement. *Phys. Rev. B*, 85:035409, Jan 2012.

[59] Marcello Calvanese Strinati, Fabrice Gerbier, and Leonardo Mazza. Spin-gap spectroscopy in a bosonic flux ladder. *New Journal of Physics*, 20(1):015004, 2018.

[60] BK Stuhl, H-I Lu, LM Aycock, D Genkina, and IB Spielman. Visualizing edge states with an atomic bose gas in the quantum hall regime. *Science*, 349(6255):1514–1518, 2015.

[61] Luca Taddia, Eyal Cornfeld, Davide Rossini, Leonardo Mazza, Eran Sela, and Rosario Fazio. Topological fractional pumping with alkaline-earth-like atoms in synthetic lattices. *Physical review letters*, 118(23):230402, 2017.

[62] Jeffrey C. Y. Teo and C. L. Kane. From luttinger liquid to non-abelian quantum hall states. *Phys. Rev. B*, 89:085101, Feb 2014.

[63] E. Tirrito, M. Rizzi, G. Sierra, M. Lewenstein, and A. Bermudez. Renormalization group flows for wilson-hubbard matter and the topological hamiltonian. *Phys. Rev. B*, 99:125106, Mar 2019.

[64] Matteo M. Wauters and Giuseppe E. Santoro. Quantization of the hall conductivity in the harper-hofstadter model. *Phys. Rev. B*, 98:205112, Nov 2018.

[65] Fan Yang, Vivien Perrin, Alexandru Petrescu, Ion Garate, and Karyn Le Hur. From topological superconductivity to quantum hall states in coupled wires. *Physical Review B*, 101(8):085116, 2020.